This is the accepted manuscript made available via CHORUS. The article has been published as:

Low-frequency coupled modes in disordered Pb(Zr,Ti)O_{3} solid solutions from first principles

Jeevaka Weerasinghe, Dawei Wang, and L. Bellaiche

Phys. Rev. B **85**, 014301 — Published 17 January 2012

DOI: 10.1103/PhysRevB.85.014301

Low-frequency coupled modes in disordered Pb(Zr,Ti)O_3 solid solutions from first principles

Jeevaka Weerasinghe,[1,*] and Dawei Wang,[2,1] and L. Bellaiche[1]
[1]*Physics Department, University of Arkansas, Fayetteville, Arkansas 72701, USA and*
[2] *Electronic Materials Research Laboratory, Key Laboratory of the Ministry of Education and International Center for Dielectric Research, Xi'an Jiaotong University, Xi'an 710049, China*

The low-frequency (< 80cm^{-1}) optical modes appearing in the dielectric spectra at low temperature are determined across the morphotropic phase boundary of disordered Pb(Zr,Ti)O_3 solid solutions from the use of first-principles-based molecular dynamics simulations. In particular, the number of these modes, their resonant frequencies and dielectric spectral weights are obtained for any Ti composition ranging between 45% and 56% – which, according to the simulations, allows the existence of three different equilibrium phases all exhibiting both *long-range-ordered* ferroelectric motions and oxygen octahedral tiltings, that are of rhombohedral $R3c$, monoclinic Cc and tetragonal $I4cm$ space groups. In particular, a compositional-induced anticrossing occurring within the bridging Cc state is revealed, and the difference in frequency between A' and A'' modes in the Cc state is linked to a quantity introduced here and termed the monoclinic depth. Moreover, the coupling between ferroelectric degrees of freedom and oxygen octahedral tiltings is found to play a crucial role on the characteristics of the low-frequency optical modes in the $R3c$, Cc and $I4cm$ phases. Analytical models are further developed to reproduce and better understand such characteristics.

PACS numbers: 63.20.K-, 63.20.dk, 63.50.Gh, 77.84.Cg, 77.80.bg, 77.22.Ch

I. Introduction

Perovskite alloys of the form (A′A″) (B′B″)O_3 are of high technological interest because of their unusual properties[1–4]. For instance, Pb($Zr_{1-x}Ti_x$)O_3 (PZT) solid solutions possess large electromechanical coupling coefficients within a narrow range of Ti compositions that defines the so-called morphotropic phase boundary (MPB) region. As a result, PZT systems are widely used in piezoelectric transducers and actuators[2,3]. The technological interest of PZT has led to intense scientific investigation in order to better understand its properties. Consequently, monoclinic phases have been recently reported in the morphotropic phase boundary of PZT[5–12], and it has been proposed that the composition-induced rotation of the polarization occurring within these low-symmetry phases is the mechanism that is responsible for the large values of the piezoelectric coefficients[13,14]. Other recent findings in the MPB area concern the observation and/or prediction of low-temperature structural phases that exhibit long-range-ordered ferroelectric (FE) motions coexisting with long-range-ordered oxygen octahedral tiltings (note that these latter tiltings are also commonly termed antiferrodistortive (AFD) motions). For instance, the rhombohedral $R3c$ state is well established to occur at low temperature in the Ti-poorer compositional side of the MPB[7,9,15,16]. On the other hand, the prediction of a tetragonal $I4cm$ state occurring in the Ti-richer compositional side of the MPB[17] is consistent with some measurements[12,15,18] while it has not been observed through other experiments[19]. Similarly, the existence of a pure monoclinic Cc state in the compositional range located in-between the $R3c$ and $I4cm$ states is currently subject to debate. As a matter of fact, some studies report such monoclinic phase[9,10,12,15] while others do not[18–20].

As indicated by Refs.[15,21–23], one key signature of the co-existence of long-range-ordered FE and AFD motions is the doubling (with respect to phases that are "only" ferroelectric) of the number of low-frequency optical modes that can be seen in the Raman or dielectric spectra – because of a coupling between ferroelectric degrees of freedom and oxygen octahedral tiltings. Determining the number of such modes and their characteristics (such as their resonant frequency and spectral weight) as a function of composition in the MPB of PZT can thus significantly help in resolving controversies about the symmetry of the low-temperature phases in this important solid solution. However, such determination can be rather challenging to extract from measurements because the peaks associated with these modes may easily overlap[24,25] and one needs many samples in order to carefully scan the MPB area. Having simulations that are able to predict the compositional dependencies of these low-frequency modes' characteristics at low temperature may thus be beneficial to the ferroelectric community. *Understanding* such compositional dependencies in terms of, e.g., the coupling between FE and AFD motions is also of obvious fundamental importance.

The aim of this work is two-fold. First of all, we wish to conduct first-principles-based simulations to predict some characteristics of the low-frequency (< 80cm^{-1}) optical modes that can appear in the dielectric and Raman spectra at low-temperature across the morphotropic phase boundary of disordered PZT solid solutions. Secondly, we want to develop analytical models that are able to reproduce such characteristics for any composition lying inside the MPB, in order to better understand the role of coupling between FE and AFD motions on such characteristics.

This paper is organized as follows. Section II details our effective-Hamiltonian-based molecular dynamics (MD) approach to obtain the low-frequency modes' characteristics in the MPB region of PZT. In Sec. III, we present and discuss the results of our MD simulations. Analytical models are introduced in Sec. IV to help gain further insight into the MD results. Finally, Sec. V provides a summary and conclusions of the present work.

II. Methods

Here, we use the effective Hamiltonian scheme of Ref. [17] to investigate Pb(Zr,Ti)O_3(PZT) solid solutions. Its total energy is written as:

$$\begin{aligned} E_{\text{tot}} &= E_{\text{FE}}\left(\{\boldsymbol{u}_i\},\{\boldsymbol{v}_i\},\{\eta_H\},\{\sigma_j\}\right) \\ &+E_{\text{AFD}}\left(\{\boldsymbol{\omega}_i\},\{\boldsymbol{v}_i\},\{\eta_H\},\{\sigma_j\}\right) \\ &+E_C\left(\{\boldsymbol{u}_i\},\{\boldsymbol{\omega}_i\}\right) \end{aligned} \quad (1)$$

where $\boldsymbol{u}_i$ denotes the local soft mode in the unit cell *i*. This local soft mode is centered on the B-sites, is directly proportional to the electric dipole at the cell i, and is associated with the lowest transverse optical (TO) phonon branch; $\{\boldsymbol{v}_i\}$ are dimensionless displacement variables, which are centered on Pb sites and are used to calculate the inhomogeneous strain tensor[26]. $\{\eta_H\}$ is the homogeneous strain tensor, which allows the simulation supercell to vary in size and shape. σ_j characterizes the atomic configuration, with σ_j=+1 or -1 corresponding to the presence of a Zr or Ti atom, respectively, at the B-lattice site *j*[14]. $\boldsymbol{\omega}_i$ is a (B-centered) vector characterizing the direction and magnitude of the AFD motions in unit cell *i*[17]. For instance, $\boldsymbol{\omega}_i = 0.1\hat{\mathbf{k}}$ corresponds to a rotation of 0.1 radians about the z-axis (when denoting $\hat{\mathbf{k}}$ the unit vector along the z-axis). E_{FE} gathers the energy terms solely involving the local soft mode, strain and their mutual couplings[14]. E_{AFD} contains energies involving the AFD motions and their couplings with strain. E_C characterizes the interaction between FE and AFD degrees of freedom. It is of particular relevance to our investigation since it heavily influences the low-frequency modes arising from such interaction[21,22] . E_C is given by[17]:

$$E_C\left(\{\boldsymbol{u}_i\},\{\boldsymbol{\omega}_i\}\right) = \sum_i \sum_{\alpha,\beta,\gamma,\delta} D_{\alpha\beta\gamma\delta}\boldsymbol{\omega}_{i,\alpha}\boldsymbol{\omega}_{i,\beta}\boldsymbol{u}_{i,\gamma}\boldsymbol{u}_{i,\delta} \quad (2)$$

where *i* runs over all the unit cells, $\alpha,\beta,\gamma,$ and δ denote Cartesian components, and $D_{\alpha\beta\gamma\delta}$ are coupling parameters[17]. All the coefficients of this effective Hamiltonian have been derived from first-principle calculations performed on small supercells using the plane-wave ultrasoft pseudo-potential method[27] within the local density approximation[28,29]. Previous usage of this effective Hamiltonian in Monte-Carlo (MC) simulations of disordered PZT[17] produced transition Curie temperatures that are compatible with experimental observations near the MPB[9,15]. Moreover, these computations yielded $P4mm$, $R3m$, $R3c$, and Cm states for different composition–temperature combinations, in good agreement with observation through diverse techniques – such as X-ray diffractions[7,8], neutron scattering[12], and Raman measurements[15,16,24]. Interestingly, these simulations also predicted the occurrence of a low-temperature Cc phase, which is consistent with some measurements[9,10,12,15] while in contradiction with other experiments' analysis[18–20]. The prediction of a low-temperature $I4cm$ phase also resulted from the use of this effective Hamiltonian[17], which was then confirmed in some measurements[12,15,18], although it too has not been observed through other experiments[19].

The total energy of this effective Hamiltonian scheme is used here in molecular dynamics (MD) simulations of PZT. We first equilibrate the system with a certain Ti composition at a temperature of interest by running 3×10^5 MD steps of NPT (canonical ensemble) simulations on a $12\times12\times12$ supercell (8640 atoms). Each time step is 0.5 fs. Then, the system is equilibrated at constant energy by conducting 10^5 MD steps of NVE (microcanonical ensemble) simulations. Subsequently, 6.9×10^6 NVE steps are performed to obtain time-dependent properties of the investigated system. Typical outputs of the MD simulations are the supercell average of the local mode vector, AFD vector and strain tensor components as a function of time. As in Refs. [21,22], two different complex responses are computed in the gigahertz/terahertz regime and at finite temperature, through the MD simulations. These are:

$$\begin{aligned} \varepsilon_{\alpha\beta}(\nu)-1 =& \frac{1}{\varepsilon_0 V k_B T}\left[\langle d_\alpha(t)\, d_\beta(t)\rangle \right. \\ &\left. + i2\pi\nu\int_0^\infty dt e^{i2\pi\nu t}\langle d_\alpha(t)\, d_\beta(0)\rangle\right] \\ \varepsilon^{\text{AFD}}_{\alpha\beta}(\nu)-1 =& \frac{1}{\varepsilon_0 V k_B T}\left[\langle \omega_{\alpha,R}(t)\, \omega_{\beta,R}(t)\rangle \right. \\ &\left. + i2\pi\nu\int_0^\infty dt e^{i2\pi\nu t}\langle \omega_{\alpha,R}(t)\, \omega_{\beta,R}(0)\rangle\right] \end{aligned} \quad (3)$$

where ν is the frequency, while α and β define Cartesian components. $\boldsymbol{d}(t)$ and $\boldsymbol{\omega}_R(t)$ are the dipole moment and the order parameter associated with AFD motions corresponding to the R point of the cubic Brillouin zone at time t, respectively[17,30]. "< >" indicates thermal average. $\varepsilon_{\alpha\beta}(\nu)$ is the complex dielectric response[31,32], while $\varepsilon^{\text{AFD}}_{\alpha\beta}(\nu)$ can be thought as the response of $\boldsymbol{\omega}_R(t)$ to its conjugate field – which is a staggered field[21,33]. Each peak in these two responses is fitted using classical damped harmonic oscillators of the form $\varepsilon(\nu) = S\nu_r^2/\left(\nu_r^2-\nu^2+i\gamma\nu\right)$ where ν_r, γ and S are the resonant frequency, damping constant and strength of the corresponding mode, respectively.

III. Results of the simulations

MD simulations are carried out for *disordered* PZT solid solutions, with Ti compositions ranging from 45.2% to 56.0% in intervals of 0.2% and for temperatures ranging from 1100K down to 10K. Time averaging of the MD outputs of the simulations gave the same phase transition sequences and similar transition temperatures than those obtained from the Monte-Carlo (MC) approach of Ref.[17]. Figure 1(a) provides the magnitude of the local mode vector ($|\langle\boldsymbol{u}\rangle|$) and its Cartesian components ($\langle u_x\rangle$, $\langle u_y\rangle$, and $\langle u_z\rangle$) –averaged over the MD steps and the supercell sites – as a function of composition in disordered PZT solid solutions at 10K. Note that the x-, y- and z-axes are chosen along the pseudo-cubic [100], [010] and [001] directions, respectively. Figure 1(b) provides similar information, but for the magnitude of the an-

tiphase AFD vector ($|\langle \boldsymbol{\omega}_R \rangle|$) and its Cartesian components ($\langle \omega_{x,R} \rangle$, $\langle \omega_{y,R} \rangle$, and $\langle \omega_{z,R} \rangle$). For compositions in the 45.2%-47.5% range, all components found for both local mode and AFD motions were non-zero with $\langle u_x \rangle = \langle u_y \rangle = \langle u_z \rangle$ and $\langle \omega_{x,R} \rangle = \langle \omega_{y,R} \rangle = \langle \omega_{z,R} \rangle$. This is indicative of the rhombohedral $R3c$ phase, as consistent with the measurements of Refs. [7,15,23]. Within the 47.5%-51.0% range, all components found for both local mode and AFD motions were similarly non-zero, but in this case $\langle u_z \rangle$ was larger than $\langle u_x \rangle$ and $\langle u_x \rangle = \langle u_y \rangle$, while $\langle \omega_{z,R} \rangle$ was larger than $\langle \omega_{x,R} \rangle$ and $\langle \omega_{x,R} \rangle = \langle \omega_{y,R} \rangle$. Such equalities and inequalities are consistent with a monoclinic Cc phase. Furthermore, since the ratio $\langle u_z \rangle$ / $\langle u_x \rangle$ is different from $\langle \omega_{z,R} \rangle$ / $\langle \omega_{x,R} \rangle$, the axis of rotation of the oxygen octahedra does not coincide with the direction of polarization in this Cc state. Finally, for compositions varying between 51.0% and 56.0%, $\langle u_z \rangle$ and $\langle \omega_{z,R} \rangle$ were the only non-zero components found for the local mode vector and AFD motions, respectively, indicating the occurrence of a tetragonal $I4cm$ phase. It is also interesting to realize that Figs. 1(a) and 1(b) reveal that the *magnitudes* of both the local mode vector and the antiphase AFD vector are nearly constant within the compositional range defining the Cc state. Thus, we can conclude that both polarization and AFD vectors are "simply" rotating from the [111] to the [001] pseudo-cubic direction as the overall Ti concentration increases within the Cc phase.

Furthermore, Figures 1(c) and (d) display the composition dependence of the resonant frequencies, ν_r, and the corresponding spectral weights, $S\nu_r^2$, of low-frequency modes (i.e., below 100 cm^{-1}), obtained through fittings of the frequency peaks of the dielectric responses for the same temperature of 10 K. As previously indicated in Ref. [21], we numerically find the existence of two (double degenerate) E(TO) modes – denoted by $E^{(1)}$ and $E^{(2)}$ – in the $R3c$ state, as consistent with experiments[15,16,18] conducted at low temperature. The origin of these two modes was revealed to be the coupling between the AFD and FE degrees of freedom[21]. In other words, thanks to this coupling, the AFD mode acquires some polarity and thus can be seen in the dielectric and Raman spectra, in addition to the "usual" ferroelectric E(TO) peak. As the Ti composition increases from 45%, both $E^{(1)}$ and $E^{(2)}$ modes' frequencies slightly decrease (in agreement with the measurements of Ref.[18]) and then undergo a clear splitting starting from 47.6%. This splitting is exactly coincident with the advent of the Cc phase for PZT at 10 K, as evidenced from Figs. 1(a) and 1(b). Each E mode splits into $A' + A''$ modes. Let us denote the two modes resulting from the splitting of $E^{(1)}$ as $A'^{(1)}$ and $A''^{(1)}$. Similarly, the two modes originating from $E^{(2)}$ are denoted by $A'^{(2)}$ and $A''^{(2)}$. We numerically find that the $A'^{(1)}$, $A''^{(1)}$, $A'^{(2)}$ and $A''^{(2)}$ peaks observed in the dielectric response have corresponding peaks (with identical resonant frequencies) in the $\varepsilon_{\alpha\beta}^{\text{AFD}}(\nu)$ AFD response. This proves that these four modes all possess both FE and AFD characters, thanks to the couplings between these two different structural degrees of freedom. Moreover, computing the tensor components of $\varepsilon_{\alpha\beta}(\nu)$ and $\varepsilon_{\alpha\beta}^{\text{AFD}}(\nu)$ in a new basis where the z-axis is along the polarization reveals that all these modes correspond to electric dipole oscillations being perpendicular to the direction of polarization in the Cc phase. Furthermore, Fig. 1(c) indicates that the frequency difference between the $A'^{(1)}$ and $A''^{(1)}$ (and also between $A'^{(2)}$ and $A''^{(2)}$) is relatively small in the Cc state. For instance, these differences are typically smaller than the frequency difference between $E^{(1)}$ and $E^{(2)}$ in the $R3c$ phase. Figure 1(c) further shows that these frequency differences between the A' and A'' modes originating from $E^{(1)}$ and $E^{(2)}$, to be denoted by $\Delta\nu(E^{(1)})$ and $\Delta\nu(E^{(2)})$, respectively, are largest near the compositional mid-point of the Cc phase (that is located around a Ti composition of 49.4 %) and decrease to either side of it. To better understand and quantify this point, let us introduce a parameter quantifying how far away is a Cc state with respect to its delimiting $R3c$ and $I4cm$ "borders". Here, this parameter is denoted by m_{dep}, is termed the "monoclinic depth", and is defined by:

$$m_{\text{dep}} = \frac{\left(\hat{\boldsymbol{P}}.\hat{\boldsymbol{m}}\right)\left(\hat{\boldsymbol{\omega}}.\hat{\boldsymbol{m}}\right)}{\left(\hat{\boldsymbol{P}}.\hat{\boldsymbol{\omega}}\right)} - \cos^2\theta_m \qquad (4)$$

where $\hat{m}$ is the unit vector along the direction that equally divides the [001] and [111] pseudo-cubic directions. As a result, $\hat{\boldsymbol{m}} = \frac{\hat{\boldsymbol{i}}+\hat{\boldsymbol{j}}+\left(1+\sqrt{3}\right)\hat{\boldsymbol{k}}}{\sqrt{2\sqrt{3}\left(1+\sqrt{3}\right)}}$, with $\hat{\boldsymbol{i}}$, $\hat{\boldsymbol{j}}$ and $\hat{\boldsymbol{k}}$ being the unit vectors along the pseudo-cubic [100], [010] and [001] directions, respectively. In Eq.(4), $\hat{\boldsymbol{P}}$ and $\hat{\boldsymbol{\omega}}$ are the unit vectors along the direction of polarization and along the axis about which the long-range-ordered oxygen octahedra tilt, respectively. θ_m is the polar angle of $\hat{\boldsymbol{m}}$, therefore yielding $\cos^2\theta_m = \frac{1+\sqrt{3}}{2\sqrt{3}}$. Note that Eq.(4) ensures that m_{dep} is zero in the $R3c$ and $I4cm$ phases and equal to $\frac{\sqrt{3}-1}{2\sqrt{3}}$ if $\hat{\boldsymbol{P}}$ and $\hat{\boldsymbol{\omega}}$ both lie along $\hat{\boldsymbol{m}}$. Figure 2 displays $\Delta\nu(E^{(1)})$ and $\Delta\nu(E^{(2)})$ *versus* m_{dep} within the Cc compositional region and at 10 K, as well as their fittings by polynomials of first or second order. One can indeed see that $\Delta\nu(E^{(1)})$ and $\Delta\nu(E^{(2)})$ can be reasonably well fitted by these polynomials. Interestingly, these polynomials are monotonically increasing functions of the "monoclinic depth", which therefore quantitatively confirms that the closer the Cc state is from its mid-point (between the $R3c$ and $I4cm$ phases), the larger are the frequency splittings. In Fig. 1(d), the sum of the spectral weights of $A'^{(1)}$ and $A''^{(1)}$, and the sum of of the spectral weights of $A'^{(2)}$ and $A''^{(2)}$, are plotted in the Cc phase (along with the spectral weight of the $E^{(1)}$ and $E^{(2)}$ modes in the $R3c$ and $I4cm$ phases), as a function of composition. Such figure reveals that, at the rhombohedral "border" of this monoclinic phase, the strength of the $E^{(1)}$ mode is larger than that of the $E^{(2)}$ mode, while the $E^{(2)}$ becomes much more polar with respect to $E^{(1)}$ at the "tetragonal" compositional border of the Cc phase. This change in polarity occurs via the gain in the sum of the spectral weights of $A'^{(2)}$ and $A''^{(2)}$ at the expense of the sum of the spectral weights of $A'^{(1)}$ and $A''^{(1)}$, when the Ti composition increases within the Cc state. Figure 1(e) further shows

that, conversely, the modes derived from $E^{(2)}$ (i.e., $A'^{(2)}$ and $A''^{(2)}$) lose more and more their AFD character during that compositional increase, while the modes that are originating from $E^{(1)}$ strengthen their AFD character. Such features are indicative of a compositionally-induced *anticrossing* (between the "bare" FE and AFD modes) occurring within the Cc phase. Note that an anticrossing between the $E^{(1)}$ and $E^{(2)}$ modes were previously predicted for a specific composition in the $R3c$ state of PZT[21], but it was generated by an electric field – which contrasts with the presently reported one which is induced by the composition in the Cc phase of PZT.

Figure 1(c) further indicates that the splittings of both the $E^{(1)}$ and $E^{(2)}$ modes into $A' + A''$ modes start to disappear for a composition around 51%, which is coincidentally in the vicinity of the Cc to $I4cm$ phase transition at 10K (see Figs. 1(a) and 1(b)). As a result, in the $I4cm$ phase and as consistent with symmetry, *doubly-degenerated* $E^{(1)}$ and $E^{(2)}$ modes are again observed – exactly as in the (Ti-poorer) $R3c$ phase and in agreement with recent spectroscopic observations[12,15,18]. Thus the symmetry of these modes for all low temperature phases across the MPB are consistent with predictions from group theory. Nevertheless, the frequency difference between these two modes is larger in the $I4cm$ phase than in the $R3c$ phase, and further increases when increasing the Ti composition within the $I4cm$ state (as also seen in the measurements of Ref.[18]). Furthermore, the spectral weight of $E^{(2)}$ in the dielectric spectra increases while the spectral weight of $E^{(1)}$ significantly reduces until almost vanishing when the Ti concentration increases in the $I4cm$ phase (see Fig. 1(d)).

IV. Analytical models

To understand features found in the previous section via the use and analysis of our atomistic effective Hamiltonian technique, let us develop analytical models for structural phases (such as $R3c$, $I4cm$ and Cc) that exhibit both long-range ordered FE and AFD motions. In such cases, these motions at site i can be represented as:

$$\begin{cases} \mathbf{u_i}\left(\mathbf{t}\right) = \langle \mathbf{u} \rangle + \tilde{\mathbf{u}}_\mathbf{i}\left(\mathbf{t}\right) \\ \boldsymbol{\omega}_\mathbf{i}\left(\mathbf{t}\right) = \langle \boldsymbol{\omega}_\mathbf{R} \rangle + \tilde{\boldsymbol{\omega}}_\mathbf{i}\left(\mathbf{t}\right) \end{cases} \tag{5}$$

where t represents time, $\langle \mathbf{u} \rangle$ and $\langle \boldsymbol{\omega}_\mathbf{R} \rangle$ are the equilibrium, spontaneous values of the FE and AFD motions, respectively. Finally, $\tilde{\mathbf{u}}_\mathbf{i}$ and $\tilde{\boldsymbol{\omega}}_\mathbf{i}$ are the deviations of the FE motions and AFD motions at site i, respectively, from their equilibrium values. It can be then shown, by plugging Eq.(5) into Eq.(2), that the essential FE-AFD *linear* coupling energetic term that influences the dynamics of $\tilde{\mathbf{u}}_\mathbf{i}$ and $\tilde{\boldsymbol{\omega}}_\mathbf{i}$ has the following form:

$$H_{\text{FE-AFD}} \simeq \sum_i \kappa \left|\langle \boldsymbol{u} \rangle\right| \left|\langle \boldsymbol{\omega_R} \rangle\right| \tilde{\mathbf{u}}_\mathbf{i} \cdot \tilde{\boldsymbol{\omega}}_\mathbf{i}, \tag{6}$$

where the "| |" symbol represents the magnitude of a vector, and where κ is a coupling coefficient involving the $\mathrm{D}_{\alpha\beta\gamma\delta}$ parameters of Eq.(2). Note that the precise combination of the $\mathrm{D}_{\alpha\beta\gamma\delta}$ coefficients yielding the κ parameter is different between the $R3c$, Cc and $I4cm$ states since it depends on the direction of the polarization.

A. IV. a. In case of the R3c and I4cm states

Equation (6) implies that, for the doubly-degenerate E modes of the $R3c$ and $I4cm$ states, the dynamical *coupled* equations for $\tilde{\mathbf{u}}_\mathbf{i}$ and $\tilde{\boldsymbol{\omega}}_\mathbf{i}$ are given within the harmonic approximation by:

$$\begin{cases} \frac{d^2\tilde{\mathbf{u}}_\mathbf{i}}{dt^2} + 4\pi^2\nu_u^2\tilde{\mathbf{u}}_\mathbf{i} + \frac{\kappa\left|\langle \boldsymbol{u} \rangle\right|}{m_u}\left|\langle \boldsymbol{\omega_R} \rangle\right|\tilde{\boldsymbol{\omega}}_\mathbf{i} = & \frac{Z^*\mathbf{E(t)}}{m_u} \\ \frac{d^2\tilde{\boldsymbol{\omega}}_\mathbf{i}}{dt^2} + 4\pi^2\nu_\omega^2\tilde{\boldsymbol{\omega}}_\mathbf{i} + \frac{\kappa\left|\langle \boldsymbol{u} \rangle\right|}{m_\omega}\left|\langle \boldsymbol{\omega_R} \rangle\right|\tilde{\mathbf{u}}_\mathbf{i} = & 0 \end{cases} \tag{7}$$

where ν_u and ν_ω are natural frequencies of the "bare" FE soft mode and "bare" AFD mode respectively. m_u, m_ω are the effective masses of the "bare" FE mode and the "bare" AFD mode, respectively. Z^* is the Born effective charge associated with the FE soft mode and $\boldsymbol{E}\left(t\right)$ is an applied *ac* electric field.

One important information resulting from Eq. (7) is that the dynamical coupling between the FE and AFD motions is reduced (respectively, vanishes) as the $\left|\langle \boldsymbol{\omega_R} \rangle\right|$ magnitude of the spontaneous AFD motion decreases (respectively, is annihilated). This explains why the spectral weight of the $E^{(1)}$ mode diminishes in the dielectric spectra as the Ti composition increases in the $I4cm$ state (see Fig. 1(d)). In other words, the $E^{(1)}$ mode does not have significant polarity anymore for large compositions in the $I4cm$ state (and thus can not be easily seen in the dielectric spectra) because the dynamical coupling between FE and AFD motions is rather small there as a result of small $\left|\langle \boldsymbol{\omega_R} \rangle\right|$.

Moreover, let us assume that, within the $R3c$ or $I4cm$ phase, the compositional dependencies of the natural frequencies of the "bare" FE and AFD modes are given by:

$$\begin{cases} \nu_u^2 = & (\nu_u^{(0)})^2 + fx \\ \nu_\omega^2 = & (\nu_\omega^{(0)})^2 + ax \end{cases} \tag{8}$$

where x is the Ti composition, and where $\nu_u^{(0)}$, f, $\nu_\omega^{(0)}$ and a are composition-independent parameters within the $R3c$ or $I4cm$ phase.

For small magnitude of the ac electric field, one can prove that combining Eqs. (7) and (8) provides two resonant frequencies (whose associated peaks should be seen in both the dielectric and AFD responses and that both correspond to doubly-degenerate E modes) that are given by:

$$\begin{cases} (\nu_1)^2 = & \frac{(\nu_u^{(0)})^2+(\nu_\omega^{(0)})^2}{2} + \left(\frac{a+f}{2}\right)x - \sqrt{\left(\frac{(\nu_u^{(0)})^2-(\nu_\omega^{(0)})^2}{2} + \frac{(f-a)x}{2}\right)^2 + \frac{(\kappa|\langle \boldsymbol{u}\rangle||\langle \boldsymbol{\omega_R}\rangle|)^2}{16\pi^4 m_u m_\omega}} \\ (\nu_2)^2 = & \frac{(\nu_u^{(0)})^2+(\nu_\omega^{(0)})^2}{2} + \left(\frac{a+f}{2}\right)x + \sqrt{\left(\frac{(\nu_u^{(0)})^2-(\nu_\omega^{(0)})^2}{2} + \frac{(f-a)x}{2}\right)^2 + \frac{(\kappa|\langle \boldsymbol{u}\rangle||\langle \boldsymbol{\omega_R}\rangle|)^2}{16\pi^4 m_u m_\omega}} \end{cases} \quad (9)$$

Interestingly and as shown by Fig. 1(c), Equations (9) can fit very well the resonant frequency of the $E^{(1)}$ and $E^{(2)}$ modes for all the investigated compositions in the $R3c$ and $I4cm$ phases – which validates the relevance of our analytical model based on the coupling between FE and AFD degrees of freedom. Note that, as expected, a different set of parameters (κ, $\nu_u^{(0)}$, f, $\nu_\omega^{(0)}$, a) has to be used to fit the data of the $R3c$ *versus* $I4cm$ states.

B. IV. b. In case of the Cc state

In the Cc state, the degeneracy of both $E^{(1)}$ and $E^{(2)}$ modes has been lifted, giving $A'^{(1)}$ and $A''^{(1)}$ from $E^{(1)}$ and $A'^{(2)}$ and $A''^{(2)}$ from $E^{(2)}$, as discussed previously. As indicated by our MD data (see Fig. 2), this lifting is related to the monoclinic depth introduced earlier. As inferred from Fig. (2), we can thus assume that the frequencies of the $A'^{(1)}$, $A''^{(1)}$, $A'^{(2)}$ and $A''^{(2)}$ modes are given, respectively, by:

$$\begin{cases} \nu_1' = & \nu_1 + f_1(m_{dep}) \\ \nu_1'' = & \nu_1 - f_1(m_{dep}) \\ \nu_2' = & \nu_2 + f_2(m_{dep}) \\ \nu_2'' = & \nu_2 - f_2(m_{dep}) \end{cases} \quad (10)$$

where ν_1 and ν_2 are given by Eq.(9) – and are thus solutions of the *coupled* Eqs(7) – and where f_1 and f_2 are second-order and first-order polynomials respectively, of m_{dep}. As can be seen in Fig. 1(c), these equations fit nicely the resonant frequencies of all $A'^{(1)}$, $A''^{(1)}$, $A'^{(2)}$ and $A''^{(2)}$ modes in the Cc phase for a given set of parameters (κ, $\nu_u^{(0)}$,f, $\nu_\omega^{(0)}$, a) and for given f_1 and f_2 functionals (note that we use here the m_{dep} value provided by the MD data for each Ti composition ranging within the Cc state). Such good fits further confirm the validity of our analytical models, in general, and the role of the coupling between FE and AFD motions on characteristics of low-optical phonon modes, in particular.

V. Conclusions

In summary, our first-principles-based effective Hamiltonian approach is used within MD simulations to simulate the compositional dependency of the low-frequency optical modes' characteristics in the $R3c$, Cc and $I4cm$ states across the MPB of PZT at low temperature. Examples of such characteristics are the number of these modes, their resonant frequencies and spectral weights in the dielectric and AFD spectra. In particular, a compositional-induced anticrossing is predicted to occur in the Cc state, and the polarity of one mode is expected to significantly decreases and nearly vanishes when increasing the Ti composition within the $I4cm$ state. A lifting of degeneracy of E modes into $A' + A''$ modes is also occurring in the Cc state (as consistent with group theory), with the resulting difference in frequency being related to a quantity that we denote here as the monoclinic depth and that involves the directions of the polarization and AFD vector. We further developed analytical models that are based on the linear coupling between FE and AFD motions in structural phases exhibiting both long-range-ordered polarization and oxygen octahedra tiltings. Such analytical models are able to accurately reproduce characteristics of the low-frequency optical modes, and led to a better insight into the significant role played by the coupling between ferroelectric and AFD degrees of freedom on such characteristics.

We hope that our present study will help in resolving some current controversies related to the phase diagram near the MPB of PZT, by identifying the precise symmetry of the low-temperature phases via the determination of low-frequency optical modes' characteristics. We are also confident that the present work can lead to a better understanding of the effect of coupling between different structural order parameters on dynamics of ferroelectrics[34].

We thank E. Buixaderas and J. Hlinka for very useful discussions. This work is financially supported by NSF grants DMR-1066158 and DMR-0701558. We also thank the Department of Energy, Office of Basic Energy Sciences, under contract ER-46612, and ONR Grants N00014-11-1-0384 and N00014-08-1-0915 for discussions with scientists supported by these grants. D.W. acknowledges support from the National Natural Science Foundation of China under Grant No. 10904122. Some computations were also made possible thanks to the MRI grant 0722625 from NSF and ONR Grant N00014-07-1-0825 (DURIP).

* Electronic address: jweerasi@uark.edu

[1] K. Uchino, Piezoelectric Actuators and Ultrasonic Motors (Kluwer Academic, Boston, 1996).

[2] S.-E. Park and T. R. Shrout, J. Appl. Phys. 82, 1804 (1997).

[3] O. Auciello, J. F. Scott, and R. Ramesh, Phys. Today 51, No. 7, 22 (1998).

[4] M. E. Lines and A. M. Glass, Principles and Applications of Ferroelectrics and Related Materials (Clarendon Press, Oxford, 1977).

[5] B. Noheda, D. E. Cox, G. Shirane, J. A. Gonzalo, L. E. Cross, and S.-E. Park, Appl. Phys. Lett. 74, 2059 (1999).

[6] B. Noheda, D. E. Cox, G. Shirane, S. E. Park, L. E. Cross, and Z. Zhong, Phys. Rev. Lett. 86, 3891 (2001).

[7] B. Noheda, J. A. Gonzalo, L. E. Cross, R. Guo, S.-E. Park, D. E. Cox, G. Shirane, Phys. Rev. B61, 8687(2000).

[8] B. Noheda, Curr. Opin. Solid StateMater. Sci. 6, 27 (2002).

[9] B. Noheda, L. Wu, and Y. Zhu, Phys. Rev. B 66, 060103 (2002).

[10] D. I. Woodward, J. Knudsen, and I. M. Reaney, Phys. Rev. B 72, 104110 (2005).

[11] R. Ranjan, Ragini, S. K. Mishra, D. Pandey, and B. J. Kennedy, Phys. Rev. B 65, 060102 (2002).

[12] F. Cordero, F. Craciun, C. Galassi, Phys. Rev. Lett. 98, 255701 (2007).

[13] H. Fu and R.E. Cohen, Nature (London) 403, 281 (2000).

[14] L. Bellaiche, A. Garcı´a, and D. Vanderbilt, Phys. Rev. Lett. 84, 5427 (2000); Ferroelectrics 266, 41 (2002).

[15] M. Deluca, H. Fukumura, N. Tonari, C. Capiani, N. Hasuike, K. Kisoda, C. Galassi, and H. Harima, J. Raman Spectros. 42, 488 (2010).

[16] G. Fraysse, J. Haines, V. Bornand, J. Rouquette,M. Pintard, Ph. Papet, S. Hull, Phys. Rev. B 77, 064109 (2008).

[17] I. A. Kornev, L. Bellaiche, P.-E. Janolin, B. Dkhil, and E. Suard, Phys. Rev. Lett. 97, 157601 (2006).

[18] E. Buixaderas, D. Nuzhnyy, J. Petzelt, Li Jin, and D. Damjanovic, Phys. Rev. B. 84, 184302 (2011).

[19] H. Yokota, N. Zhang, P.A. Thomas, and A.M. Glazer, Ferroelectrics 414, 147 (2011).

[20] D. Phelan, X. Long, Y. Xie, Z.-G. Ye, A. M. Glazer, H. Yokota, P. A. Thomas, and P. M. Gehring, Phys. Rev. Lett. 105, 207601 (2010).

[21] D. Wang, J. Weerasinghe, L. Bellaiche, and J. Hlinka, Physical Review B 83, 020301(R) (2011).

[22] D. Wang, E.Buxideras, J. Íñiguez, J. Weerasinghe, H. Wang, and L. Bellaiche, Phys. Rev. Lett. 107, 175502 (2011).

[23] D. B¨auerle and A. Pinczuk, Solid State Commun. 19, 1169 (1976).

[24] K. C. V. Lima, A. G. Filho, A. P. Ayala, J. Mendes Filho, P. T. Freire, F. E. Melo, E. B. Arajo, and J. A. Eiras, Phys. Rev. B 63, 184105 (2001).

[25] J. Rouquette, J. Haines, V. Bornand, M. Pintard, Ph. Papet, J. L. Sauvajol, Phys. Rev. B73, 224118 (2006).

[26] W. Zhong, D. Vanderbilt, and K. M. Rabe, Phys. Rev. Lett. 73, 1861 (1994); Phys. Rev. B 52, 6301 (1995).

[27] D. Vanderbilt, Phys. Rev. B 41, R7892(1990).

[28] L. Bellaiche and D. Vanderbilt, Phys. Rev. B 61, 7877 (2000).

[29] P. Hohenberg and W. Kohn, Phys. Rev. 136, B864 (1964); W. Kohn and L. J. Sham, ibid. 140, A1133 (1965).

[30] The order parameter of AFD motions is defined as $\langle \omega_R \rangle = \frac{1}{N} \sum_i \omega_i \left(-1\right)^{n_x(i)+n_y(i)+n_z(i)}$ where ω_i characterizes the AFD distortion in unit cell *i*, and $n_\alpha(i)$ are integers locating cell *i*.

[31] I. Ponomareva, L. Bellaiche, T. Ostapchuk, J. Hlinka, and J. Petzelt, Phys. Rev. B 77, 012102 (2008).

[32] J. M. Caillol, D. Levesque, and J. J. Weis, J. Chem. Phys. 85, 6645 (1986).

[33] Phase Transitions and Critical Phenomena, edited by C. Domb and M. S. Green (Academic, New York, 1972), Vol. I-V.

[34] A recent work[18] also mentioned the possibility of the existence of a low-frequency central mode arising from Pb hoppings (and which transforms into anti-phase Pb motions as the temperature is decreased), in addition to the modes studied here. Such central mode was experimentally considered in order to better fit infrared reflectivity measurements. We do not see such central mode in our MD simulations, either because such mode may occur in a ceramic (rather than in a single-crystal, as studied here) or because our effective Hamiltonian approach does not incorporate antiferroelectric Pb motions.

FIGURE CAPTIONS

Figure 1: (Color online) Predicted compositional dependency of some physical properties in disordered PZT at 10K. Panel (a) shows the magnitude and Cartesian components of the local mode. Panel (b) displays the same information than Panel (a), but for the AFD vector. Panel (c) provides the resonant frequency of the lowest optical phonon modes seen in the dielectric spectra. Panel (d) gives the spectral weight of the $E^{(1)}$ and $E^{(2)}$ modes in the R3c and I4cm states, as well as, the sum of the spectral weights of the $A'^{(1)}$ and $A''^{(1)}$ modes and the sum of the spectral weights of the $A'^{(2)}$ and $A''^{(2)}$ modes for the *dielectric spectra* of the Cc phase. Panel (e) is similar to Panel (d) but only for the Cc state and for the $\varepsilon_{\alpha\beta}^{\text{AFD}}(\nu)$ *AFD* response. The solid lines in Panel (c) provides the fitting of the resonant frequencies by Eqs. (9) in the $R3c$ and $I4cm$ states and by Eqs. (10) in the Cc phase.

Figure 2: (Color online) Difference in frequency between the A' and A" modes derived from the $E^{(1)}$ (in blue) and $E^{(2)}$ (in red) modes, as a function of the monoclinic depth (see text). The solid lines represent fit of these data by linear and quadratic functions in case of $\Delta\nu(E^{(2)})$ and $\Delta\nu(E^{(1)})$, respectively.

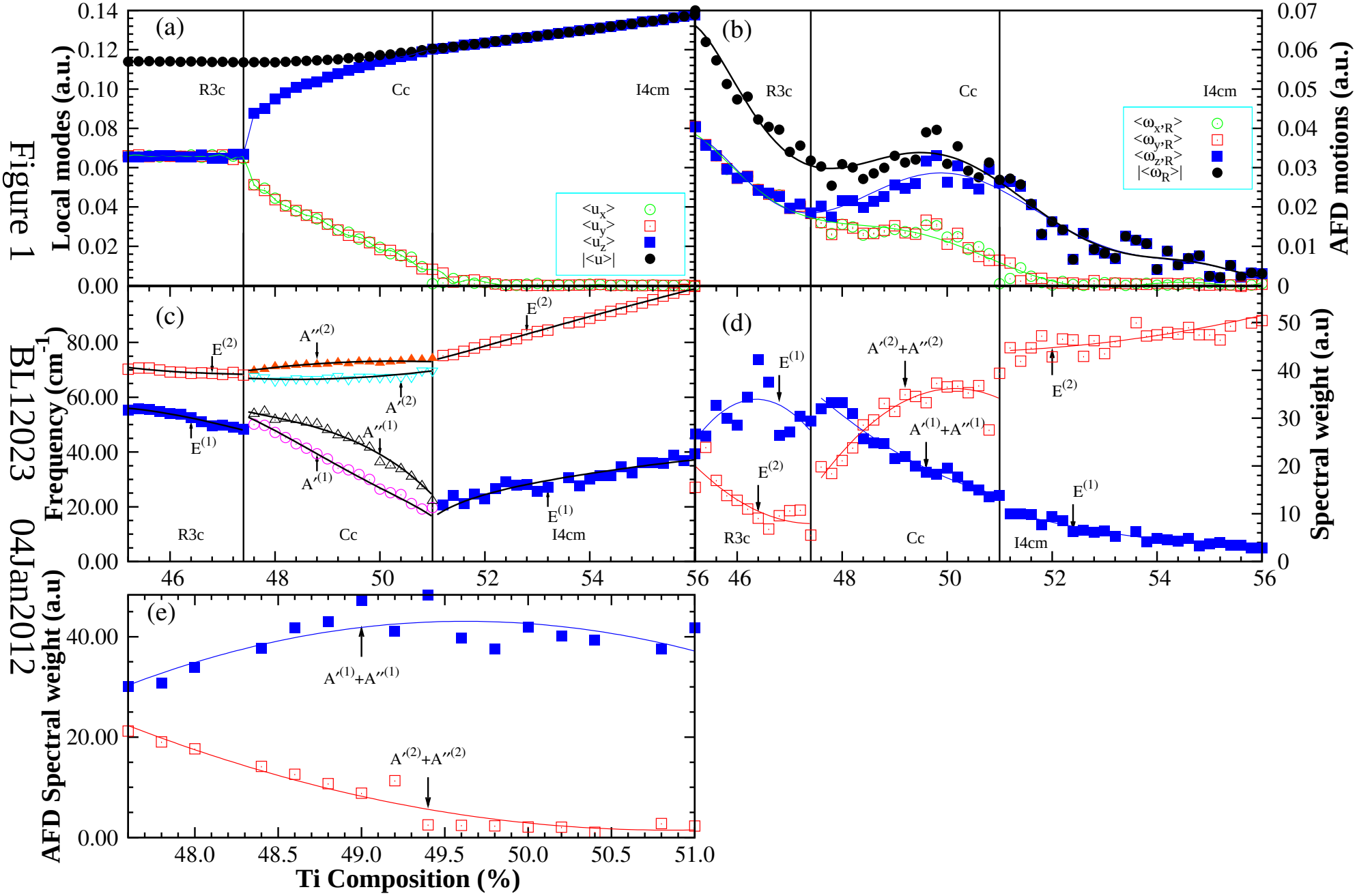

Figure 1

BL12023 04Jan2012

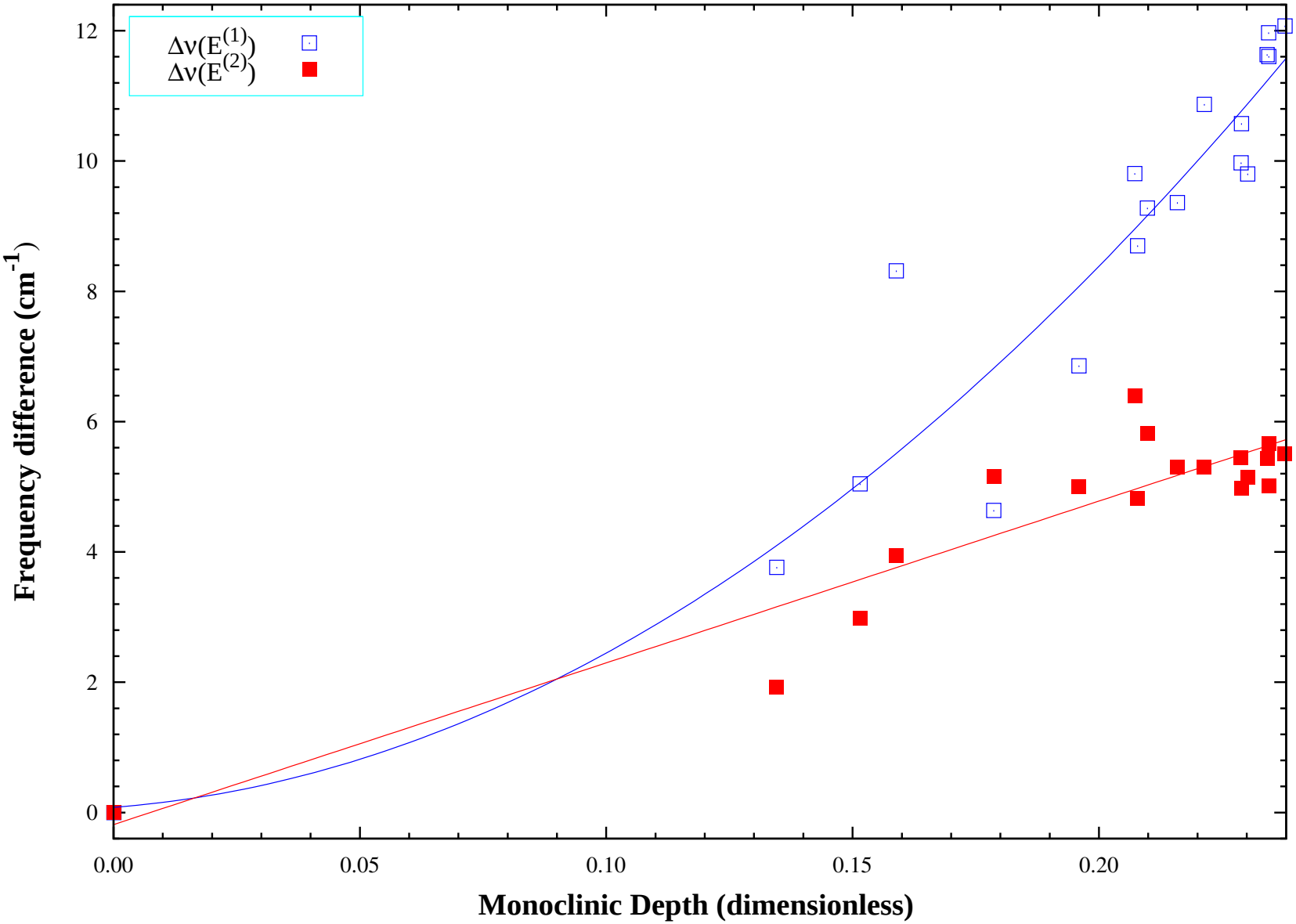

Figure 2 BL12023 04Jan2012